Exploratory Studies of the Helicity Difference in Double-Polarization Photo-Production at Jefferson Laboratory

An undergraduate thesis presented

by

Randall Evan McClellan

to

The Department of Physics

in partial fulfillment of the requirements

for receiving

Honors in the Major

Florida State University

Tallahassee, Florida

April 2009

Thesis advisor
Volker Crede

Author
Randall Evan McClellan

Abstract

The study of the excited states of the nucleon is an old field, however there is much still to discover. It is expected that photo-production experiments, polarization experiments in particular, will reveal previously unseen information about some of these excited states. The CEBAF Large Acceptance Spectrometer (CLAS) at Jefferson Laboratory is an excellent instrument for detecting the charged decay particles from photo-production reactions. In addition, the FROzen Spin Target (FROST) provides a polarized proton target which allows for an unprecedented look at double-polarization reactions.

This study covers calibrating the Drift Chambers of CLAS and exploring the helicity difference in $\gamma p \rightarrow n\pi^+$ reactions. During the course of this study, methods were developed that can be applied to many properties of numerous reactions.

Calibration of the CLAS detector components is a major task that has required the efforts of the entire run group for over a year since data taking was completed in February of 2008. Calibration software had to be learned and tested before it could be applied to the data. Then, the slow process of iteratively improving the quality of the calibrations could begin. Preliminary physics analyses with more complete sets of data have begun recently once the calibration reached a satisfactory level of quality.

The analysis developed in this project serves four purposes: making cuts so that only the desired data is used, calculating unknown quantities, removing background from the results, and producing histograms of these results. To facilitate background removal, data were taken simultaneously on three different targets: Butanol (the main polarized proton target), Carbon, and Polyethylene. Therefore, a vertex cut is necessary to choose the location from which a reaction originated, thus allowing differentiation between the three target materials. Also, cuts are made that ensure only particles which were actually involved in a physics event are used in the analysis, as CLAS can detect some non-interacting particles as well. Momentum and velocity cuts provide particle identification and decay channel selection. The next step of the analysis program is to calculate unmeasurable quantities. For this study, the important quantity is the 4-vector of the missing decay particles, the neutron. It

is unmeasurable because CLAS can only detect charged particles. Missing mass plots were generated that showed a clear neutron peak and a broad but unmistakable Δ peak over some background.

The real physics results are the helicity difference in the reaction $\gamma p \rightarrow n\pi^+$ for different incoming photon energies. They show a clear deviation from zero, indicating that the double-polarization has an effect, and polarization observables will be able to be determined in future analysis. The full determination of the polarization observables goes beyond the scope of this work, and would be an excellent project for a Ph.D. thesis.

Contents

Chapter 1

Introduction

1.1 Motivation for Polarized Photo-Production

The internal structure of the nucleon is still not completely understood. While it is known that the nucleon must be made up of smaller components, the structure and some properties of the nucleon are still a mystery. Though the Lagrangian of the underlying theory, Quantum Chromo-Dynamics, cannot be solved for bound states, many theoretical models exist to describe the internal structure and make predictions about the excited states of the nucleon. Many of these models predict states above 2 GeV that have not been confirmed, or even hinted at, by experiment. Figure 1.1 shows the predicted states of a constituent quark model[1] versus current experimental findings.

This discrepancy between model predictions and experimental findings may be explained in a few ways. First, quark models based on three constituent quark degrees of freedom are inappropriate, and the internal structure of the nucleon is too complex. In this case, current and future experiments will show evidence of excited states that differ greatly from theoretical predictions. Another possibility is that the model predictions are right, but past experiments have been unable to confirm the so-called "missing" or unobserved states due to the difficulty in identifying baryon resonances, or because they were not produced. These possibilities are what this experiment hopes to explore by using a different experimental setup and higher energies.

Just like the study of light being emitted or absorbed by electrons in atoms gives an insight into the structure of the atom, studying transitions of exited nucleon states can yield information about the internal structure of the nucleon. However, unlike atomic

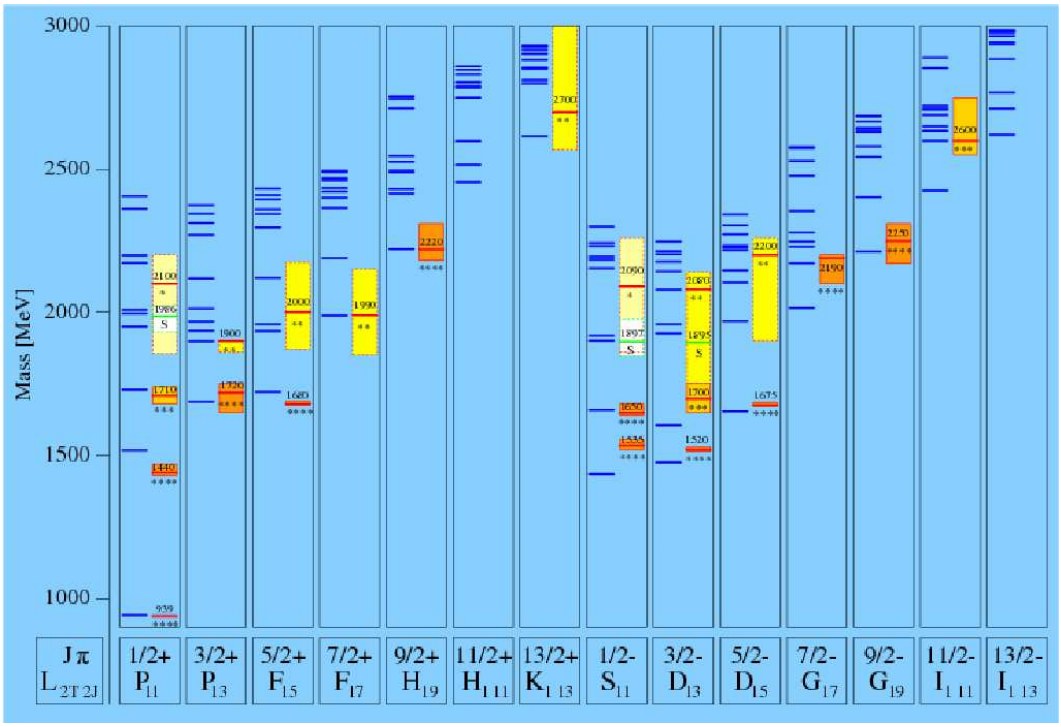

Figure 1.1: Spectrum of excited states of the nucleon. Blue lines on the left of each column are model predictions[1], boxes to the right of each column are experimental findings. Height of boxes shows range of mass measurements. Star ratings are given by the particle data group [2]. More stars means a higher confidence in the measured state.

energy transitions which produce discrete, easily distinguishable lines, baryonic transitions give broad, overlapping peaks, due to the extremely short lifetimes of the excited states. In order to disentangle any specific resonance contribution, it must be carefully extracted from the unidentified background of other contributions. This is impossible to do cleanly without limiting the possible resonances by applying clever constraints in the experiment.

For this reason, it is important to place constraints on these experiments to limit ambiguities in the data description. For this thesis, circularly-polarized photons ($\rightarrow$) were incident on longitudinally-polarized protons ($\Rightarrow$). In low enough energy ranges that orbital angular momentum has no contribution, the helicity difference polarization observable $\frac{\rightarrow\Rightarrow - \rightarrow\Leftarrow}{\rightarrow\Rightarrow + \rightarrow\Leftarrow}$ can be used to selectively excite only resonances with certain spins, limiting the number of possible resonance contributions. The majority of previous meson-production experiments have been done using pion beams. By striking protons with photons instead, we hope to find baryon resonances that may have been previously undiscovered due to weak coupling

Measurements	$p(\gamma, p)\pi^0$	$p(\gamma, \pi^+)n$
unpolarized	76 %	70 %
single-polarized	22 %	27 %
double-polarized	2 %	3 %

Table 1.1: Relative weight of unpolarized and polarized data in the current world database for pion photoproduction up to $E_\gamma = 2.0$ GeV.

to pion-nucleon interactions. In addition, the use of a polarized photon beam on a polarized proton target will result in double-polarization observables that are unprecedented in this type of measurement. These observables should limit the ambiguities and make identification of resonance contributions more accessible. Furthermore, using these data in a coupled-channel analysis with a large number of final states will hopefully lead to the identification of new and poorly measured resonances.

1.2 Motivation for $n\pi^+$

Many recent and upcoming experiments will measure polarization (or spin) observables for photo-production processes involving baryon resonances. It is clear from examining different model analyses, e.g. MAID and SAID, that differences between the predictions for these polarization observables can be large, and therefore they provide strong constraints on the analysis.

An interesting question is whether it is possible to design a complete set of experiments which will uniquely determine the scattering amplitude for a given process. In the absence of such complete sets of measurements, the inclusion of data on polarization observables into coupled-channel analysis fits is likely to have strong effects on the extracted parameters for resonances at higher energies.

While a formally complete experiment requires the measurement, at each energy and angle, of at least eight observables [3], the current database for pion photo-production is populated mainly by unpolarized cross sections. Table 1.1 shows this quite nicely. Above the second resonance region ($W = 1520$ MeV), the existing database is quite sparse, with few experiments covering large angular ranges at fixed energies. The distribution of available

$\pi^+ n$ data is given in Fig. 1.2. The polarized cross section for $\gamma \mathrm{p} \rightarrow \mathrm{n}\pi^+$ is given by,

$$\begin{aligned}\frac{d\sigma}{d\Omega} = \sigma_0\{1 - \delta_l \mathbf{\Sigma cos2}\phi + \Lambda_x(-\delta_l \mathbf{H sin2}\phi + \delta_\odot \mathbf{F}) \\ - \Lambda_y(-\mathbf{T} + \delta_\mathbf{l}\mathbf{P cos2}\phi) \\ - \Lambda_z(-\delta_l \mathbf{G sin2}\phi + \delta_\odot \mathbf{E})\}\end{aligned}$$

where $\mathbf{\Sigma}$, $\mathbf{H}$, $\mathbf{F}$, $\mathbf{T}$, $\mathbf{P}$, $\mathbf{G}$, and $\mathbf{E}$ are the observables. δ_l and $\delta_\odot$ are the longitudinal and circular degrees of beam polarization, respectively. Λ_x, Λ_y, and Λ_z are the degrees of target polarization in three directions. σ_0 is the unpolarized cross-section. No data are available for the observable F and the helicity difference E. The goal of this thesis work is to extract very preliminary results for E. The full analysis goes beyond the scope of this thesis, but will eventually greatly constrain partial-wave analyses and reduce model-dependent uncertainties in the extraction of nucleon resonance properties, providing a new benchmark for comparisons with QCD-inspired models, e.g. constituent quark models.

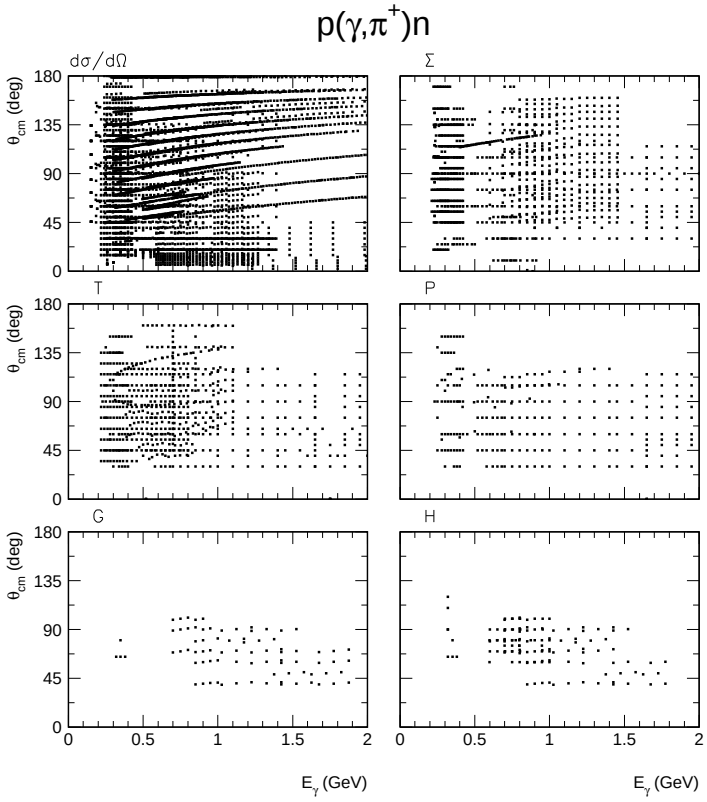

Figure 1.2: Available cross section and beam-target polarization measurements for the reaction $\gamma p \to n\pi^+$ up to 2 GeV. No data are available for the observables E and F.

Chapter 2

Experimental Setup

2.1 Introduction

2.2 CEBAF-Continuous Electron Beam Accelerator Facility

The Thomas Jefferson National Accelerator Facility in Newport News, Virginia is home to the Continuous Electron Beam Accelerator Facility (CEBAF). CEBAF provides electron beams with energies up to 5.75 GeV. The electrons are accelerated in a racetrack-shape, superconducting ring before being fed to three experimental halls, seen in Figure 2.1.

For the FROST experiment, polarized electrons from CEBAF are used to create circularly and linearly polarized photons which collide with the polarized target. This thesis used the circularly polarized photon data sets.

2.3 CLAS-CEBAF Large Acceptance Spectrometer

The CEBAF Large Acceptance Spectrometer in Hall B at JLab is a state of the art tool ideal for studies involving charged particles from the decay of excited nucleon states.

After entering Hall B, the CEBAF electron beam strikes a radiator, which causes the electrons to lose energy through Bremstrahlung radiation. The resulting photons continue down the beam line toward the target, while the electrons are diverted by a magnetic field, according to their energy loss, into the tagger. The tagger is a set of scintillation counters that measures the energy of the electrons and records the time that they were measured. Meanwhile, the photons are striking the Frozen Spin Target (FROST), which

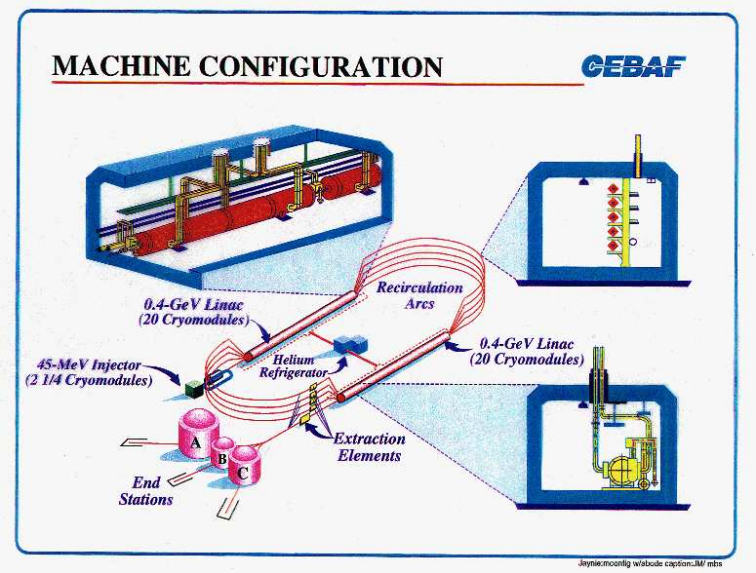

Figure 2.1: CEBAF schematic. The FROST Experiment took place in Hall B.

will be discussed in the next section. After the reaction takes place, the decay particles first pass through the Start Counter which immediately surrounds the target. The Start Counter serves as a first-level trigger and records initial timing information that, combined with information from the tagger, helps to associate a reaction with a specific CEBAF electron. Thus, the energy of the specific photon that caused the reaction is known, or "tagged".

Next, the decay particles pass into the Drift Chambers, large chambers containing trapped gas and parallel wires throughout. Any charged decay particles leave an ion trail in the gas that is detected by the sense wires. Because of the magnetic field created by the toroidal magnets within the chambers, charged particles will feel a Lorentz force and leave curved tracks through the drift chambers. Positive particles are curved outward, away from the beam line. The purpose of the drift chambers is to measure the momentum of charged particles; the curvature of the particle tracks allows for precise determination of the momentum. Beyond the Drift Chambers is the Time Of Flight Counter (TOF). The TOF records the time it takes for the particles to travel from the start counter to the TOF. This time determines velocity and energy. With all of these components together, the charged decay particles can be identified and their 4-vectors can be determined completely. The organization of the large components of CLAS are seen in Figure 2.2.

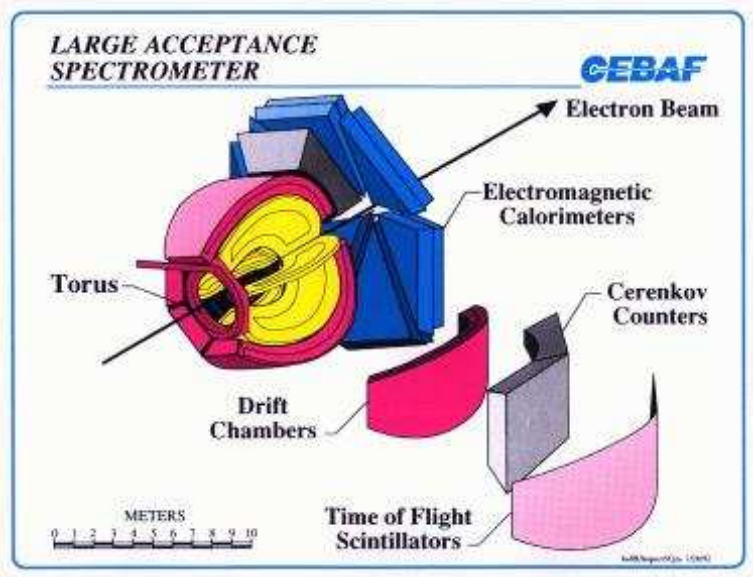

Figure 2.2: CLAS setup in Hall B. For the FROST run period, a photon beam was used, not an electron beam.

2.4 FROST-FROzen Spin Target

A polarized proton target is central to the purpose of this experiment. However, it is not easy to accomplish. Since the use of hydrogen is impractical due to polarization complications, a different target material must be used. Butanol (C_4H_9OH) is a good compromise between resistance to radiation damage, a long relaxation time, and a high dilution factor of about 13.5%. The dilution factor is the ratio of polarizable protons to unpolarizable nucleons in the Butanol target. Butanol has ten hydrogen atoms, the protons of which can be polarized. So, there are ten polarized protons for every seventy-four nucleons. This is further complicated by the fact that all of the other nucleons in butanol, because they are bound in nuclei, are subject to Fermi motions which yield very broad resonances that add background to the measurements. Therefore, FROST was designed with three targets at different distances down the beam line. First is the frozen spin butanol target. Following it are two smaller targets: one is a disk of pure carbon (graphite) to study bound nuclei, and the other is a plastic disk made of polyethylene (CH_2) to study unpolarized hydrogen. These extra targets will provide a means of subtracting out unwanted effects from the true polarized data.

The polarized protons slowly lose their polarization over time, so re-polarization must

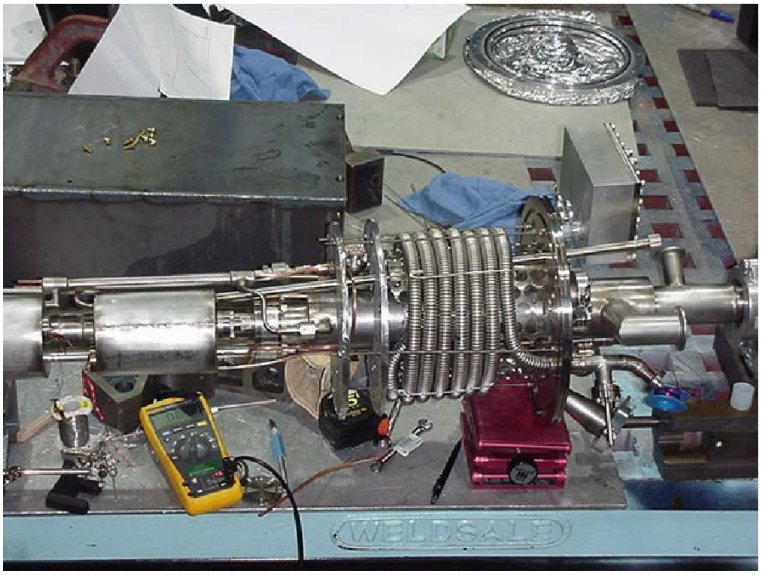

Figure 2.3: A picture of the FROST Pre-Cooler. The actual target is out of view to the left.

occur occasionally. However, the target spin was flipped throughout the experiment to study systematic effects, and re-polarization coincided with spin-flipping, so no beam time was lost for re-polarization. Polarization is done through a series of steps that involve removing the target from the detector. The target is first held at 0.3 K in an external polarizing magnetic field of 5 Tesla. This field polarizes the free radicals from the atoms of a doping material, TEMPO. Then, a microwave generator is applied near the ESR frequency to transfer the polarization of the electrons to the protons. The microwave is turned off, and then the target is cooled to a temperature of 30 mK. The FROST pre-cooler is seen in Figure 2.3. At this temperature, the polarization of the protons is effectively frozen, hence the name of the target. The target-mounted holding magnet is then turned on, producing a field of 0.5 Tesla. At this point, the target is returned to the detector, and measurements can continue.

For this experiment, the target was always polarized longitudinally. The polarization switched between parallel and anti-parallel to the beam line. A complimentary experiment is planned for 2009/2010 which will use transverse target polarization.

Chapter 3

Calibration

3.1 Introduction

The calibration of all the detector components of CLAS is a huge undertaking that has required the cooperation of the entire run group and over a year of work. The main focus of the calibration that must be done before analysis can start is on the tagger, the Time of Flight detectors (TOF), the Start Counter (ST), the Drift Chambers (DC), and the electromagnetic calorimeters (EC). The calibration of each of these components was taken charge of by members of the run group. Weekly meetings ensured that progress was always being made and that all discussions included everyone involved in calibration. My first assignment in working on this experiment was to learn the procedure and programs involved in calibration of the Drift Chambers, and to apply what I had learned once the TOF calibration was good enough to allow work to begin on DC.

3.2 Drift Chambers

The Drift Chambers can be loosely thought of as a hexagonal onion, as can be seen in Figure 3.1. Assuming that 'down the beam line' is the positive z direction, then there are six sectors, each covering one sixth of the azimuthal angle and extending from 0 to π in the polar angle. Each of these is divided up radially into three regions, with region one closest to the beam line. Furthermore, each region is made up of two superlayers. The superlayers are labeled similarly to the regions, superlayer one is closest to the beam line, superlayer six is the outermost. Finally, each superlayer is made up of six, radially stacked layers of

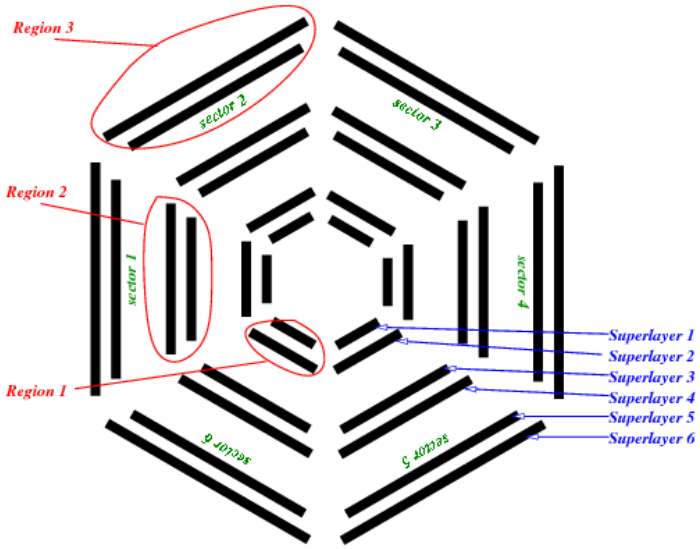

Figure 3.1: Cross section of the Drift Chambers in the plane normal to the beam line. Each line represents one superlayer of wires.

sense wires. However, due to spacial restrictions, superlayer one only contains four layers. Regions one and three are essentially free of any magnetic field, but region two sits around the toroidal magnet cryostats, leading to a magnetic field that bends the tracks of charged particles as they pass through this region. Positive particles are bent away from the beam line, negative ones toward it.

The calibration of the Drift Chambers that is done for each experiment is the "Time-to-Distance" calibration. This is the relationship between the drift time and the distance of closest approach of the reconstructed particle path to a specific sense wire. A sample of this calibration is shown in Figure 3.2. This would be fairly simple if the electric field around each sense wire were cylindrically symmetric and if each particle passing through produced identical ionization. However, neither of these are true. Each sense wire has six neighbor field wires. So, the electric field becomes hexagonal toward the edge of each cell. This is even further complicated in Region 2, where the toroidal magnets warp the electric field so that even a hexagon does not approximate the shape of the cell very well. The fact that not all tracks produce identical ionization requires the determination of a time-walk correction during the Drift Chamber Calibration.

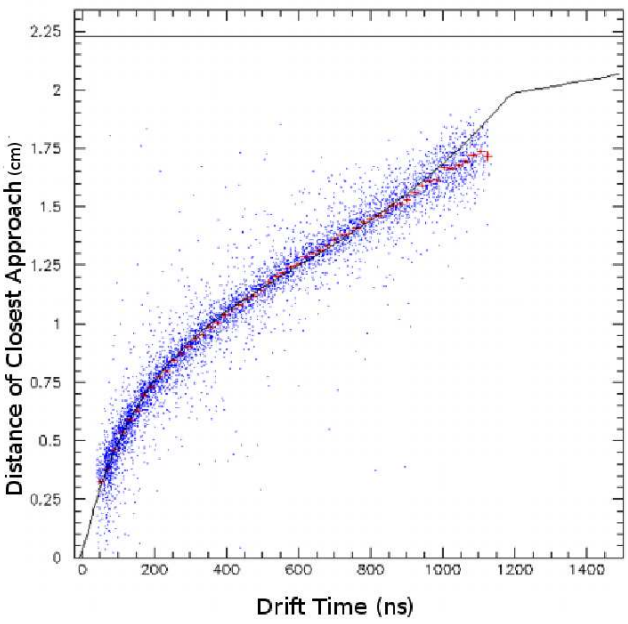

Figure 3.2: Example of a fitted time to distance calibration plot. The fitted line represents the relationship between drift time and the closest distance from the sense wire to the reconstructed track

3.3 Status

After data taking was completed, the entire set of data was reconstructed, or "cooked" based on preliminary calibrations. This process can take up to a month, and it is called the "pass0" cooking. Then, over the next year, the collaboration members have worked on the calibration of all the detector components, occasionally recooking small subsets of the data to determine the quality of the current state of calibration. After all calibrations are satisfactorily completed, the entire data set is cooked again, yielding "pass1". At the time of the defense of this thesis, pass1 is half completed. Tremendous progress has been made in the quality of the Drift Chamber Calibrations since the beginning of pass0 (Fig. 3.3). The definition of the residuals is given by the formula: $RESIDUAL = abs(DOCA) - abs(DIST)$. $DOCA$ is the "Distance of Closest Approach" or the distance from the sense wire to the fitted particle track. $DIST$ is the calculated distance from the sense wire to the track based on measured drift time and drift velocity. A perfect calibration would make these exactly equal, giving a residual of zero.

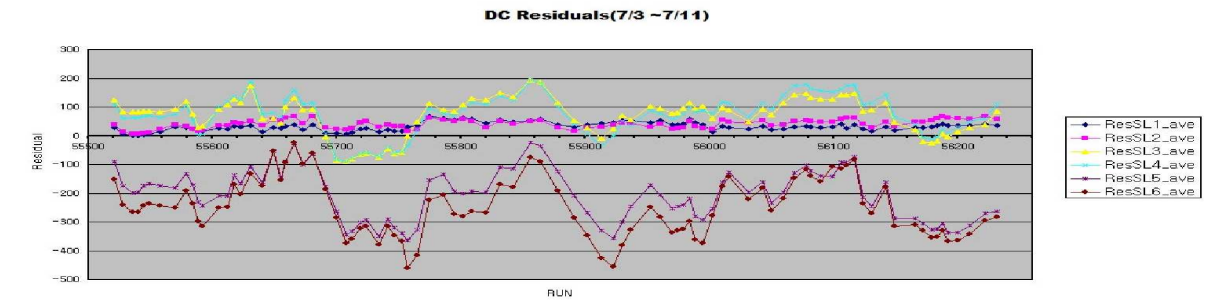

(a) Initial Average Residuals

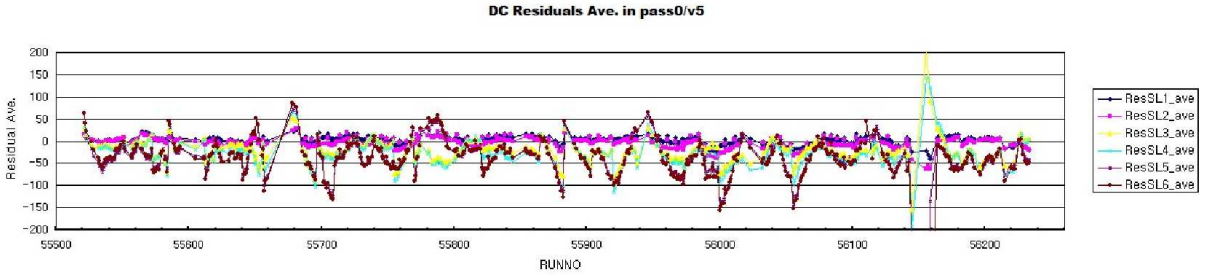

(b) Final Average Residuals

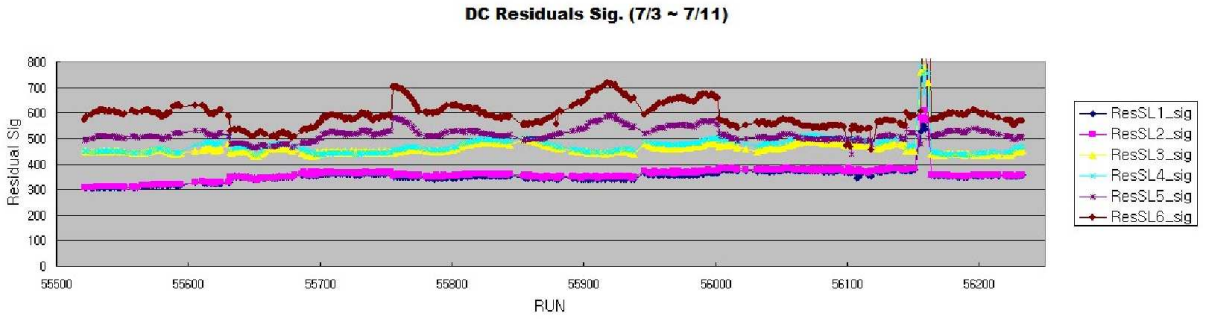

(c) Initial Residual Sigmas

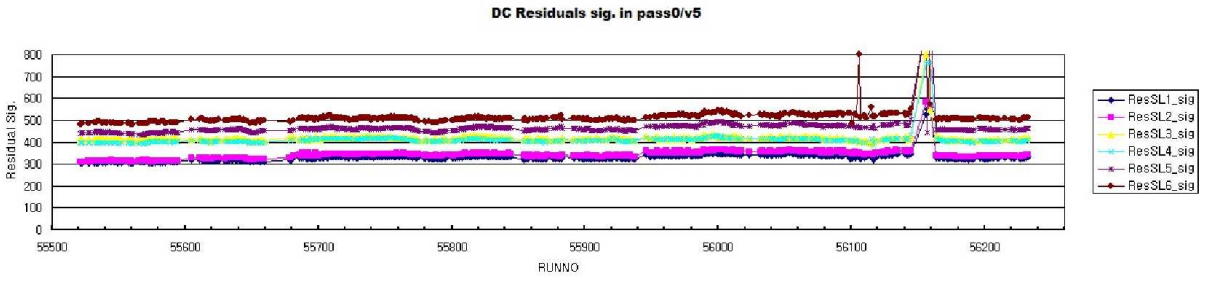

(d) Final Residual Sigmas

Figure 3.3: These plots demonstrate the improvement of the Drift Chamber Calibration from a very early stage to the quality used on the pass1 recooking.

Chapter 4

Analysis of $\gamma p \rightarrow n\pi^+$

4.1 Introduction

As the calibration finishes, physics analyses on the FROST [4] [5] [6] [7] [8] data can begin. The preliminary analysis on the calibrated data that this paper is focusing on involves studying the helicity difference in $n\pi^+$ final states. The data is read from CLAS raw data banks and the desired information is extracted using a package in ROOT[1] called ROOTBEER. ROOTBEER[2] was developed specifically for the purpose of extracting data from CLAS formatted banks. This analysis was performed by developing ROOTBEER code that would read the raw CLAS data banks, perform the preliminary analysis, and produce histograms of the relevant results.

4.2 ROOTBEER

The ROOTBEER code serves three purposes that are essential to obtain meaningful results. These are applying necessary cuts, calculating interesting quantities, and producing histograms of the results.

First, applying cuts to certain measurable quantities and choosing the right values for these cuts are critical steps in calculating good results. The simplest cut is called the 'vertex cut', and limits the region of the target where events originate. The cuts were from -4.5 cm

[1]ROOT is a system of C++ based, object-oriented frameworks created at CERN for the purpose of handling and analyzing large amounts of high-energy physics data in an efficient manner

[2]The ROOTBEER website is `http://nuclear.gla.ac.uk/~kl/rootbeer/`

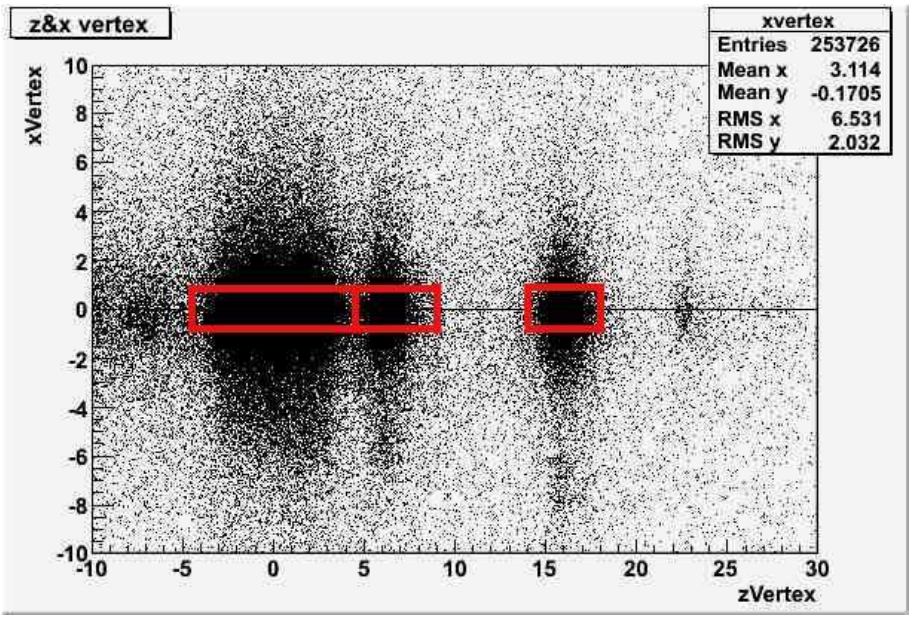

Figure 4.1: Two-dimensional plot of the target vertex. The beam-line is on the x-axis, and one perpendicular dimension is on the y-axis. The cut sections for the three targets, butanol, carbon, and polyethylene, are drawn in red.

to 4.5 cm for butanol, 4.5 cm to 9.0 cm for carbon, and 14.0 cm to 18.0 cm for polyethylene. Also, a cut was applied around the beam axis in the shape of a square with sides 1.2 cm long centered on the beam axis. A vertex plot with cuts is seen in Figure 4.1. Using this cut, data from the three targets can be analyzed independently. By calculating results using only the butanol target, and then subtracting the same results using the carbon and polyethylene targets, the background can be reduced such that only photon reactions with polarized protons are used.

Choosing the correct tagged photon is a very important cut due to the large number of potential candidate photons. Without consistently choosing the correct photon for each event, the results would be meaningless nonsense. The correct photon is determined by comparing timing information from the start counter to timing information of all the tagged photons associated with that event. Specifically, the time that all of the decay particles must have originated in the target is calculated. This time is compared with the time that all of the tagged photons passed through the target. The photon with the closest time is chosen and used for further calculation. The validity of the chosen photons can easily be seen in the missing mass plot of reconstructed neutrons. This missing mass is formed by choosing only

events with a detected π^+, and then applying the relativistic energy formula $m^2 = E^2 - p^2$ to find the invariant mass of the missing 4-vector. Because the 4-vector of the neutron is reconstructed using the energy of the beam photon, it is very sensitive to changes in the photon's energy. A distinct peak at the neutron mass indicates that the correct photon has been chosen a great majority of the time, as seen in Figure 4.2.

Another important cut is choosing only events which have a π^+ and a neutron in the decay. But first, all detected charged particles must be identified. Although this is done in the construction of the BOS[3] banks before analysis, it is important to understand how it is accomplished. As discussed before, the Drift Chambers measure the momentum of charged particles. The Time of Flight calorimeters measure the flight time, and, since we know the distance from the Start Counter to the TOF Calorimeters, the velocity of particles can be determined. Combining the velocity with the momentum, the rest mass of particles can be determined. This identifies the particles except for those with mass degeneracy, such as positive and negative pions. These are disentangled by examining the bend in their tracks through the magnetic field present in Region 2 of the Drift Chambers. The cut on one specific reaction is done by keeping track of all of the measured particles in each event, and then only using events with exactly one detected π^+, exactly zero detected protons, and exactly zero detected π^-. Then, when the missing mass of these events are calculated, the neutron at 938 $\frac{MeV}{c^2}$ and Δ at 1230 $\frac{MeV}{c^2}$ can be clearly seen above some background.

Calculating the quantities that are not directly measured, but will be needed for the production of results, is the next major purpose of the analysis code. This process begins by constructing 4-vectors of all known particles in a given reaction. This includes the chosen tagged beam photon and the target proton, as well as all measured decay particles. Then, using only π^+ events, the 4-vector of the missing particles (neutron) is reconstructed based on conservation of momentum and energy. The missing mass is then calculated, yielding a histogram with a large peak at the neutron mass, a visible delta peak, and some background. For calculation of asymmetries, a cut from 0.92 GeV to 0.97 GeV is applied to this missing mass, only a small area around the neutron peak is used.

The final data correction involved in this analysis is subtracting some of the background using the carbon target. Since butanol was used as the main target instead of pure hydrogen,

[3]BOS banks are raw reconstructed data banks that can be read by CLAS software, including ROOTBEER.

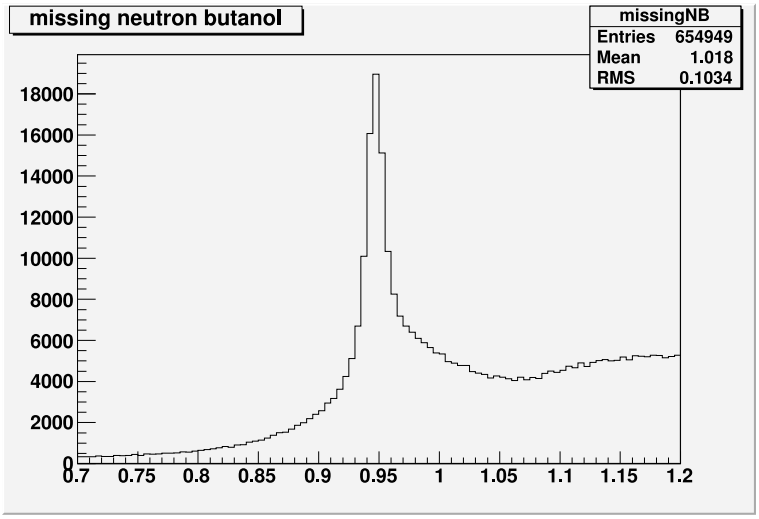

Figure 4.2: Missing Mass of γp $\rightarrow$ π^+X. Neutron peak is clearly visible. Broad Δ peak is also visible.

there is a significant amount of background due to the carbon and oxygen in the butanol molecules. This background can be dealt with for any measured or calculated quantity by finding the value for the butanol and carbon targets separately, scaling up the carbon result, and subtracting the scaled carbon value from the butanol value. The measurement from the carbon must be scaled because the carbon target is much smaller than the butanol target, and the difference in the total number of nuclei must be corrected. To find the scaling factor between the two targets, the area of the missing mass plot below the neutron peak can be used. Dividing this portion of the butanol histogram by the same section of the carbon histogram and then fitting the result to a constant value gives the scaling factor between the two targets. The effect that this background subtraction has on results is best seen in the missing mass histogram, Figure 4.3.

In addition to the missing mass histogram, the other important histogram shows the helicity difference. The helicity difference is the difference in angular distribution of the decay π^+ between events with different relative orientations of beam and target spin alignment. So, for a given orientation of target polarization, the events with positive beam helicity are subtracted from the events with negative beam helicity, this is then divided by the sum to form the asymmetry. The helicity difference is best displayed on a two-dimensional histogram of the cosine of the polar angle of the π^+ in the center of mass frame versus the energy of the tagged photon. However, since it is difficult to read numbers off of a

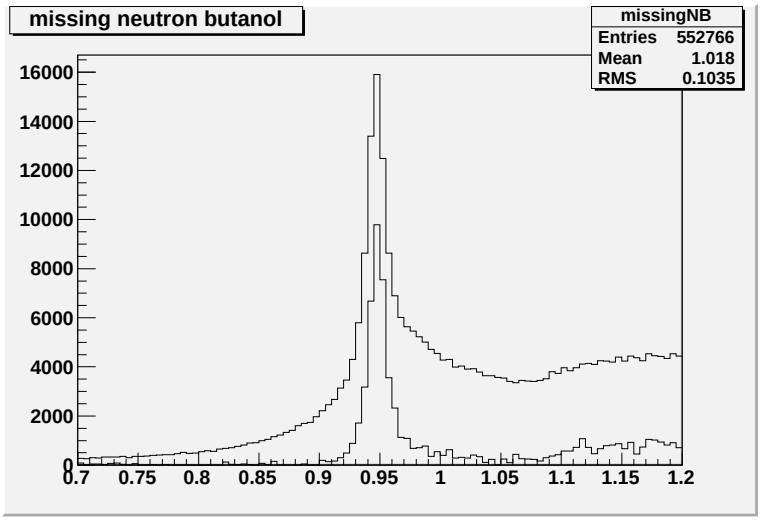

Figure 4.3: The raw and subtracted missing mass histograms for γp $\rightarrow$ π^+X. The carbon subtraction eliminates the background around the neutron peak.

two-dimensional histogram, projecting this histogram into energy bins and looking at one histogram for each energy bin is more informative, as seen in Figure 4.4.

4.3 Results

The above described analysis was run over a subsection of the data. This subset contained only data for which the photons were circularly polarized. About 0.52% of the cicularly polarized data was used in this analysis. Furthermore, only one target setup was used. The orientation of the polarization of the protons and the orientation of the holding field were both directed in the positive direction: down the beam line. The results are all presented in the histograms in this section.

The clear deviation from zero in these three histograms is the primary result of this study. The goal of this project was to determine whether or not the polarization worked, and if it was likely that polarization observables would be extractable from this data. The non-zero asymmetry answers both of these questions. Yes, the polarization worked. This data is easily distinguishable from unpolarized data. Yes, it is highly likely that future analysis will be able to determine the value of helicity related polarization observables.

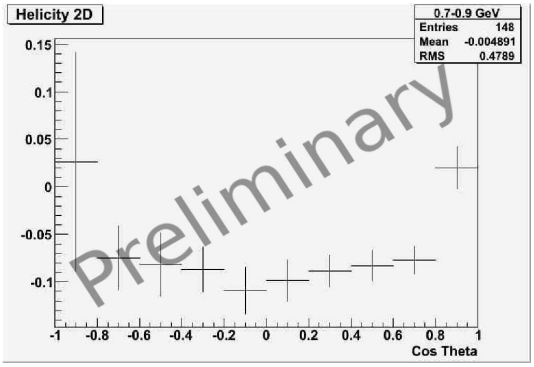

(a) No Carbon Subtraction. Photon energy range: 0.7 to 0.9 GeV

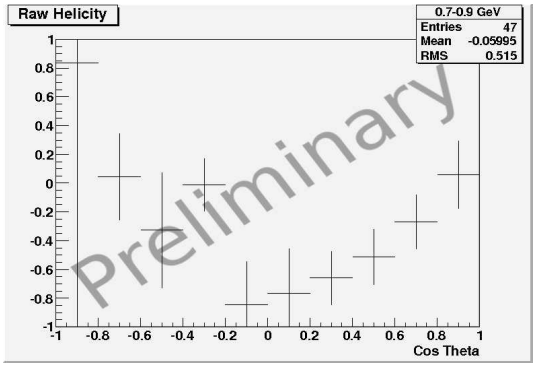

(b) Carbon Subtracted. Photon energy range: 0.7 to 0.9 GeV

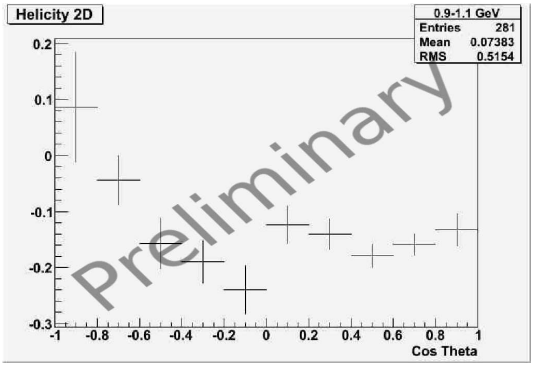

(c) No Carbon Subtraction. Photon energy range: 0.9 to 1.1 GeV

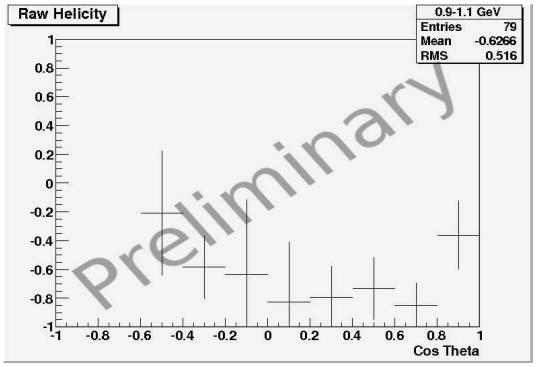

(d) Carbon Subtracted. Photon energy range: 0.9 to 1.1 GeV

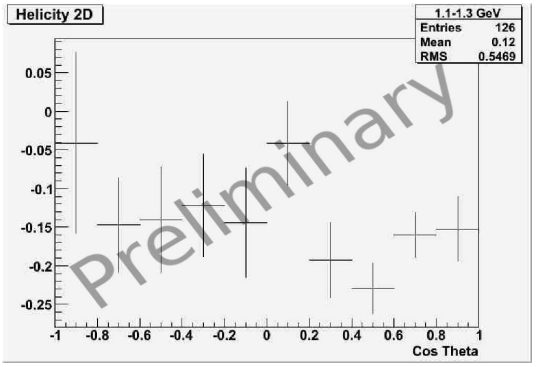

(e) No Carbon Subtraction. Photon energy range: 1.1 to 1.3 GeV

Figure 4.4: Helicity Asymmetry in cosine of the polar angle of the pion in $\gamma p \rightarrow n\pi^+$ reactions. These are all preliminary histograms. The carbon-subtracted asymmetry for 1.1 GeV and up has too much error to provide meaningful results.

Chapter 5

Summary and Outlook

As the calibration phase of this experiment draws near conclusion, full analyses on various observables in various reactions will soon begin. However, there are still a number of corrections that must be completed before analysis can be finalized. These include Energy-Loss Corrections, Momentum Corrections, and the determination of the proper covariance matrix for Kinematic Fitting. Energy-Loss Corrections account for the loss of energy that all particles experience as they travel through the supporting structures of the detector. Because this effect is not corrected for in the main calibration phase, it remains to be completed. Errors in the measured momentum of particles arise due the simplified model of the magnetic field used in the track fitting of the offline reconstruction code and the calibration of the Drift Chambers. The actual magnetic field is, of course, slightly different than what it is assumed to be during calibration. This means that momentum corrections must be calculated and applied after the calibration is done. Finally, after both of these corrections are completed, kinematic fitting can be done on all reactions. Kinematic fitting is simply shifting the value of all measured quantities within their error bars such that certain constraints, such as conservation of momentum and conservation of energy, are exactly fulfilled. This final step of data preparation provides a more perfect data set by smoothing out any remaining errors in measurements.

The future of the analysis for $\gamma p \rightarrow n\pi^+$ looks very promising. Once all the final corrections have been finished, the helicity difference can be used to selectively excite only resonance contributions with a specific spin.

Bibliography

[1] U. Loring, K. Kretzschmar, B. Metsch, and H. Petry, *"Relativistic quark models of baryons with instantaneous forces"*, Eur. Phys. J. **A10**, 309 (2001), hep-ph/0103287.

[2] C. Amsler *et al.*, Particle Data Group, *Review of particle physics*, Phys. Lett. **B667**, 1 (2008).

[3] I. Barker, A. Donnachie, and J. Storrow, *"Complete Experiments in Pseudoscalar Photoproduction"*, Nucl. Phys. **B95**, 347 (1975).

[4] F. Klein, T. Todor, and P. Eugenio, *"Search for Missing Nucleon Resonances in the Photoproduction of Hyperons using Polarized Photon Beam and Polarizd Target"*, 2002, JLab Proposal E02-112.

[5] S. Strauch, N. Benmouna, and I. Strakovsky, *"Pion Production From a Polarized Target"*, 2003, JLab Proposal E03-105.

[6] D. Sober, M. Khandaker, and D. Crabb, *"Helicity Structure of Pion Photoproduction"*, 2004, JLab Proposal E04-102.

[7] V. Crede, S. Strauch, and M. Bellis, *"Measurement of $\pi^+\pi^-$ Photoproduction in Double-Polarization Experiments using CLAS"*, 2006, JLab Proposal E06-013.

[8] E. Pasyuk and M. Dugger, *"Measurement of polarization observables in η photoproduction with CLAS"*, 2005, JLab Proposal E05-012.